
Continuous Bayesian Model Selection for Multivariate Causal Discovery

Anish Dhir*¹ Ruby Sedgwick*¹ Avinash Kori¹ Ben Glocker¹ Mark van der Wilk²

*Equal contribution

Abstract

Current causal discovery approaches require restrictive model assumptions or assume access to interventional data to ensure structure identifiability. These assumptions often do not hold in real-world applications leading to a loss of guarantees and poor accuracy in practice. Recent work has shown that, in the bivariate case, Bayesian model selection can greatly improve accuracy by exchanging restrictive modelling for more flexible assumptions, at the cost of a small probability of error. We extend the Bayesian model selection approach to the important multivariate setting by making the large discrete selection problem scalable through a continuous relaxation. We demonstrate how for our choice of Bayesian non-parametric model, the Causal Gaussian Process Conditional Density Estimator (CGP-CDE), an adjacency matrix can be constructed from the model hyperparameters. This adjacency matrix is then optimised using the marginal likelihood and an acyclicity regulariser, outputting the maximum a posteriori causal graph. We demonstrate the competitiveness of our approach on both synthetic and real-world datasets, showing it is possible to perform multivariate causal discovery without infeasible assumptions using Bayesian model selection.

1. Introduction

In many systems, for example, protein signalling networks, variables causally relate to each other as changing a variable only modifies certain variables (Sachs et al., 2005). Uncovering these unique underlying causal structures from

data can allow us to gain new insights in a wide range of fields, from Biology (Sachs et al., 2005) to Medicine (Feuerriegel et al., 2024) to Economics (Hicks et al., 1980). There are two main approaches to learning causal structures from data. The first approach assumes a restricted model class for the data generating process (Peters et al., 2017, Ch. 4), but its guarantees often fail when these assumptions don't hold. The second approach requires interventional data for all variables, which can be costly, ethically challenging, or even impossible (Li et al., 2019). Consequently, learning a unique causal structure often relies on impractical assumptions, limiting its real-world applicability.

Recent work has shown that Bayesian model selection can be used to learn a unique causal structure without interventional data while broadening the flexibility of usable model classes (Dhir et al., 2024). This comes at a cost of loosened identifiability guarantees but with the ability to posit more realistic assumptions. In fig. 1, we illustrate a causal relationship in the Sachs dataset (Sachs et al., 2005) that our less restrictive model captures accurately, while most methods assuming additive noise (ANM) fail (Hoyer et al., 2008). Figure 1(a) demonstrates that the ANM assumption is inappropriate, causing its guarantees to break down. In contrast, Bayesian model selection enables the use of models with more suitable assumptions (fig. 1(b)). However, the current formulation of Bayesian model selection for causal discovery requires computing and comparing the posteriors of all possible causal graphs. As the number of graphs grows super-exponentially with the number of variables, this approach becomes computationally intractable for large graphs.

A potential solution lies in continuous optimisation causal discovery approaches (Zheng et al., 2018). These approaches interpret causal discovery as a single optimisation problem that is amenable to gradient based methods. So far, methods making use of continuous optimisation have been limited to using restricted model classes or interventional data. In this work, we propose a scheme to extend Bayesian model selection based causal discovery to multiple variable systems using continuous optimisation — facilitating more flexible causal discovery at larger scales.

¹ Department of Computing, Imperial College London, London, UK ²Department of Computer Science, University of Oxford, Oxford, UK. Correspondence to: Mark van der Wilk <mark.vdwilk@cs.ox.ac.uk>.

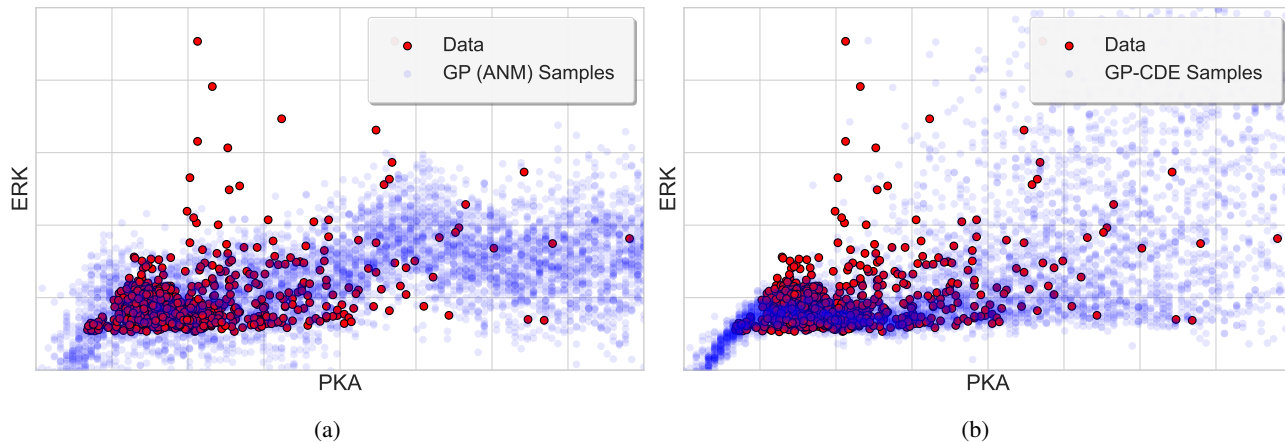


Figure 1. The figure shows model samples for the PKA \rightarrow ERK pathway from the Sachs dataset (Sachs et al., 2005). (a) Samples from a Gaussian Process (GP) with the ANM assumption. (b) Samples from the GP-CDE model. The ANM assumption is unsuitable here as it cannot capture the varying noise, whereas the GP-CDE model assumptions can.

We start with a Bayesian non-parametric model that can model non-Gaussian and heteroscedastic densities, the Gaussian Process conditional density estimator (GP-CDE) (Titsias and Lawrence, 2010; Lalchand et al., 2022). We show that certain hyperparameters of this model can be interpreted as an adjacency matrix for a graph, allowing for continuously parametrising the space of graphs. These hyperparameters can then be optimised over, using a loss derived from Bayesian model selection, and a regulariser to ensure the final adjacency represents a valid acyclic graph. Priors placed over these hyperparameters can also be interpreted as priors over graphs, leading to a scheme that returns the *maximum a-posteriori* (MAP) causal graph. We show the practical advantage of this method with competitive performance across synthetic and real datasets. Our work shows that it is beneficial in practice to give up on strict identifiability results under unrealistic assumptions for realistic assumptions, even if these imply a small but irreducible probability of error.

2. Background

Our work is concerned with recovering causal structure from data. Here, we outline material relevant to this task and the assumptions required.

2.1. Causal Model

We make the common assumption that there are no hidden confounders. We assume that data $\mathbf{X} \in \mathbb{R}^{N \times D}$ can be explained by a *Causal Model*, which we refer to as $\mathcal{M}_{\mathcal{G}}$. A causal model can be formally defined by a *directed acyclic graph* (DAG) with vertex set \mathcal{V} and edge set \mathcal{E} , denoted $\mathcal{G} = (\mathcal{V}, \mathcal{E})$, along with a set of conditional distributions $\mathcal{C} := \prod_{i \in \mathcal{V}} \mathcal{C}_{i|\text{PA}_{\mathcal{G}}(i)}$, where $\text{PA}_{\mathcal{G}}(i)$

denotes the parents of node i in \mathcal{G} , and $\mathcal{C}_{i|\text{PA}_{\mathcal{G}}(i)}$ is the set of conditionals for variable i . An element of \mathcal{C} induces a joint distribution over D random variables $X = \{X_1, \dots, X_D\}$ when its constituent members are multiplied together. That is, for $(P_i : i \in \mathcal{V}) \in \mathcal{C}$ the joint factorises as $\prod_{i=1}^D P_i(X_i | X_{\text{PA}_{\mathcal{G}}(i)})$. We denote the set of *all induced joints* as $\mathcal{F} = \{\prod_{i=1}^D P_i(X_i | X_{\text{PA}_{\mathcal{G}}(i)}) : (P_i : i \in \mathcal{V}) \in \mathcal{C}\}$ (Dhir et al., 2024). We also assume likelihood modularity (Geiger and Heckerman, 2002), that is for variable i if $\text{PA}_{\mathcal{G}}(i) = \text{PA}_{\mathcal{G}'}(i)$ for $\mathcal{G} \neq \mathcal{G}'$, then $\mathcal{C}_{i|\text{PA}_{\mathcal{G}}(i)} = \mathcal{C}_{i|\text{PA}_{\mathcal{G}'}(i)}$. This means that for graphs where variables have the same parents, we assume the same set of conditional distributions.

The causal model is assumed to satisfy the *Independent Causal Mechanism* (ICM) assumption (Janzing and Schölkopf, 2010). This states that the terms in the product $\prod_{i=1}^D P_i(X_i | X_{\text{PA}_{\mathcal{G}}(i)})$, that constitutes the factorisation according to \mathcal{G} , are composed of autonomous modules. This implies that changing one term (such as under an intervention) leaves all other terms unchanged. This property does not necessarily hold in any other factorisation of the joint (Peters et al., 2017).

As variables are dependent only on their parents in a graph by construction, a causal model satisfies the *Markov* assumption. This states that d-separations in \mathcal{G} between variables implies conditional independence between the same variables (Pearl, 2009). We also assume *faithfulness*: any conditional independences between variables are represented by d-separations in \mathcal{G} (Pearl, 2009). Together, faithfulness and Markov assumptions imply a one-to-one relationship between independences in the distributions and d-separations in the graph (Peters et al., 2017). These assumptions are enough to recover a causal structure from data up to a Markov equivalence class (MEC), that is the class of causal structures that have the same d-separations.

2.2. Learning Causal Structure

Formally, the task is to recover a DAG \mathcal{G} given a dataset of N samples with D variables, $\mathbf{X} \in \mathbb{R}^{N \times D}$. As stated in section 2.1, without any interventional data and equipped with only the faithfulness and Markov assumptions, only the MEC of a DAG can be recovered (Pearl, 2009). To recover a unique DAG, and differentiate *within* an MEC, we require additional assumptions.

2.3. Learning Causal Structure with Functional Restrictions

One way to recover a DAG is to impose prior restrictions on the allowable conditional distributions $\mathcal{C}_{i|\text{PA}_{\mathcal{G}}(i)}$. These restrictions are chosen so that the joint distributions implied by a causal model cannot be expressed by any other causal model—specifically, for $P \in \mathcal{F}_{\mathcal{G}}$ it holds that $P \notin \mathcal{F}_{\mathcal{G}'}$ for any $\mathcal{G}' \neq \mathcal{G}$ (Guyon et al., 2019, Ch. 2). Thus if data is sampled from one of the causal models, the causal structure can be identified with probability 1. Zhang et al. (2015) show that the maximum likelihood score is sufficient to identify the causal structure with these restricted models. As an example, additive noise models (ANM) (Hoyer et al., 2008) restrict all $\mathcal{C}_{i|\text{PA}_{\mathcal{G}}(i)}$ to the form $f(X_{\text{PA}_{\mathcal{G}}(i)}) + \epsilon$ for some arbitrary non-linear function f , and arbitrarily distributed ϵ . If we consider a different graph \mathcal{G}' but same restrictions on $\mathcal{C}_{i|\text{PA}_{\mathcal{G}'}(i)}$, it is not possible to approximate the joint induced by the original set of conditional distributions $\prod_{i \in \mathcal{V}} \mathcal{C}_{i|\text{PA}_{\mathcal{G}}(i)}$.

Methods relying on restricted model classes also restrict the datasets they can model. Specifically, assume that data was generated by a distribution Π , then it may be that $\Pi \notin \mathcal{F}_{\mathcal{G}}$ for all \mathcal{G} . Here, none of the causal models can approximate the true data-generating distribution and guarantees about causal identifiability no longer hold. That is, the models are misspecified. A solution would be to loosen the restrictions on $\mathcal{C}_{i|\text{PA}_{\mathcal{G}}(i)}$ providing greater flexibility in approximating distributions. However, this could also allow causal models with different DAGs to express the true data-generating distribution, thereby losing the ability to recover the true DAG (Zhang et al., 2015, Lemma 1).

2.4. Learning Causal Structure with Bayesian Model Selection

Bayesian model selection has previously been used with linear models to learn an MEC (Heckerman, 1995; Heckerman and Geiger, 1995; Heckerman et al., 1995; Geiger and Heckerman, 2002). Following other attempts (Friedman and Nachman, 2000; Stegle et al., 2010), Dhir et al. (2024) showed that Bayesian model selection can allow for distinguishing between distinct casual models even if they can express the same distribution, such as when using

non-parametric model classes. Here, the strict identifiability of restricted model classes no longer holds, although the probability of error may be small depending on the model used and can be estimated empirically (Dhir et al., 2024) (discussed further in appendix A). The advantage of this approach is that it allows for using more flexible model classes to learn causal structures, potentially mitigating the misspecification issues discussed in section 2.3, where the guarantees of restricted model classes do not hold. Our work takes advantage of these insights.

In Bayesian model selection, the evidence for a causal model $\mathcal{M}_{\mathcal{G}}$ (as defined in section 2.1) is quantified by the posterior

$$P(\mathcal{M}_{\mathcal{G}}|X) \propto P(X|\mathcal{M}_{\mathcal{G}})P(\mathcal{M}_{\mathcal{G}}), \quad (1)$$

where $P(\mathcal{M}_{\mathcal{G}})$ is the prior over the causal model. To indicate no preference over causal direction between variables, the prior is chosen to be uninformative about graphs in the same MEC. The term $P(X|\mathcal{M}_{\mathcal{G}})$ is known as the *marginal likelihood*. We select the most likely causal model $\mathcal{M}_{\mathcal{G}}^*$ based on the highest posterior value (Kass and Raftery, 1995)

$$\mathcal{M}_{\mathcal{G}}^* = \underset{\mathcal{M}_{\mathcal{G}}}{\operatorname{argmax}} P(\mathcal{M}_{\mathcal{G}}|X). \quad (2)$$

To calculate the marginal likelihood, a prior (denoted π) over the distributions in the causal model must be defined. The only constraint placed on the prior is that it should encode the ICM assumption (section 2.1) (Stegle et al., 2010; Dhir et al., 2024). The ICM assumption implies that knowledge about any distribution $P_i \in \mathcal{C}_{i|\text{PA}(i)}$ should not inform any other $P_j \in \mathcal{C}_{j|\text{PA}(j)}$ for $j \neq i$. This is achieved by defining factorised priors on each variable distribution set — $\pi_i \in \mathcal{P}(\mathcal{C}_{i|\text{PA}_{\mathcal{G}}(i)})$ where π_i is the prior on the distributions for variable i , and \mathcal{P} is the set of all distributions over an object. Given the prior, the marginal likelihood is

$$P(X|\mathcal{M}_{\mathcal{G}}) = \int \prod_{i=1}^D (P_i(X_i|X_{\text{PA}_{\mathcal{G}}(i)})\pi_i(dP_i)). \quad (3)$$

The marginal likelihood score can be interpreted as how well a prior, and the encoded ICM assumption within it, explains a given dataset (Dhir et al., 2024). The prior indicates the weight given to distributions in $\mathcal{C}_{i|\text{PA}_{\mathcal{G}}(i)}$ used to explain the data, effectively softening the hard restrictions discussed in section 2.3. As the prior is a distribution, it must also sum to one which means that, unlike maximum likelihood, it cannot equally weigh every element in $\mathcal{C}_{i|\text{PA}_{\mathcal{G}}(i)}$. This means that although multiple causal models can represent a given distribution, the prior and the encoded ICM assumption favour certain models over others—specifically, those whose prior and encoded ICM assumption align with that of the observed data.

Dhir et al. (2024) only consider Bayesian model selection for the two variable case. For a higher number of variables,

the number of DAGs grows super exponentially. This makes the procedure of comparing the marginal likelihood of all the causal models with distinct DAGs prohibitive. In this paper, we investigate the feasibility of scaling this approach for multiple variables.

2.5. Continuous Optimisation for Learning Causal Structure

Given a score (such as the likelihood or marginal likelihood) \mathcal{S} , causal structure learning can be defined as an optimisation problem over graphs (Zheng et al., 2018)

$$\mathcal{G}^* = \underset{\mathcal{G}}{\operatorname{argmax}} \mathcal{S}(\mathcal{G}) \text{ such that } \mathcal{G} \in \text{ DAGs.} \quad (4)$$

That is, finding the graph that optimises the score under the constraint that the graph must be a valid DAG. This converts causal structure learning into a single optimisation problem, tackling the scalability issue. However, ensuring that the graph is acyclic is nontrivial with gradient based methods.

Zheng et al. (2018) solve this by first encoding a graph with a weighted adjacency matrix $\mathbf{A} \in \mathbb{R}_{\geq 0}^{D \times D}$, then a measure of acyclicity is introduced

$$h(\mathbf{A}) = \operatorname{Tr}(e^{\mathbf{A}}) - D, \quad (5)$$

where $e^{\mathbf{A}}$ is the matrix exponential. The function $h : \mathbf{A} \rightarrow \mathbb{R}_{\geq 0}$ is a measure of the number of weighted directed walks that allow for returning to a starting node. Hence, $h(\mathbf{A}) = 0$ implies that there are no directed cycles in the adjacency \mathbf{A} and that the graph implied by \mathbf{A} is a valid DAG.

Equation (4) can now be written as an optimisation problem with the differentiable constraint $h(\mathbf{A}) = 0$. Zheng et al. (2018) use the augmented Lagrangian method to convert the above into a sequence of unconstrained optimisation problems (Nemirovsky, 1999). Solutions to the sequence of subproblems are solutions of the original constrained optimisation problem. Each subproblem is

$$\underset{\mathbf{A}}{\operatorname{argmax}} \mathcal{S}(\mathcal{G}^{\mathbf{A}}) - \frac{\rho_t}{2} |h(\mathbf{A})|^2 - \alpha_t h(\mathbf{A}), \quad (6)$$

where t is the problem index, ρ_t and α_t are coefficients of the method, while $\mathcal{G}^{\mathbf{A}}$ denotes a DAG \mathcal{G} with adjacency matrix \mathbf{A} . After each subproblem is solved, the coefficients are increased (see appendix B.3). A solution \mathbf{A}^* is found when $h(\mathbf{A}^*) < \epsilon$ for some convergence threshold $\epsilon > 0$.

3. CGP-CDE: Causal Gaussian Process Conditional Density Estimators

We propose a method that scales up Bayesian model selection based causal discovery by using the insights of Zheng et al. (2018) (section 2.5). We first describe the model that we use, then we show how the model can continuously

parameterise the space of graphs. This is followed by a loss function that maximises the posterior probability and ensures that the final graph is a DAG.

3.1. The GP-CDE Model

The Bayesian model selection approach to causal structure learning described in section 2.4 requires defining distributions and priors for a causal model. To take advantage of the Bayesian framework, we wish to use a model for each $\mathcal{C}_{i|\text{PA}_{\mathcal{G}}(i)}$ that is more flexible than previous attempts. For this, we use a version of the *Gaussian process conditional density estimator* (GP-CDE) model (Dutordoir et al., 2018).

The input to the estimator for each variable is determined by the causal graph of the causal model. For a given causal DAG \mathcal{G} , the joint $p(\mathbf{X}, \mathbf{f}, \mathbf{W} | \mathbf{A}, \phi, \mathcal{M}_{\mathcal{G}})$ of our model is

$$\prod_{i=1}^D \prod_{n=1}^N p(x_{ni} | \mathbf{f}_i, \phi_i) p(\mathbf{f}_i | \mathbf{X}_{\text{PA}_{\mathcal{G}}(i)}, \mathbf{\Lambda}_i, w_{ni}) p(w_{ni}), \quad (7)$$

where $\mathbf{W} \in \mathbb{R}^{N \times D}$ are the latent variables, $\phi \in \mathbb{R}^D$ are the likelihood variances, $\mathbf{\Lambda}_i$ are the kernel hyperparameters, and $\mathcal{M}_{\mathcal{G}}$ denotes the causal model with DAG \mathcal{G} . Each variable \mathbf{x}_i is modelled as the output of a function \mathbf{f}_i , with the parents of the variable in \mathcal{G} , $\mathbf{X}_{\text{PA}_{\mathcal{G}}(i)}$, and a latent variable \mathbf{w}_i being the inputs. The inclusion of $\mathbf{w}_i \sim \mathcal{N}(\mathbf{0}, \mathbf{I})$ allows for each variable to be described with non-Gaussian and heteroscedastic noise, greatly increasing the expressivity of the model (Dutordoir et al., 2018). The term $p(\mathbf{f}_i | \mathbf{X}_{\text{PA}_{\mathcal{G}}(i)}, \mathbf{\Lambda}_i, w_{ni})$ is the Gaussian process prior (Rasmussen, 2003), and equal to

$$\mathcal{N}(\mathbf{0}, K_{\mathbf{\Lambda}_i}((\mathbf{X}_{\text{PA}_{\mathcal{G}}(i)}, \mathbf{w}_i), (\mathbf{X}_{\text{PA}_{\mathcal{G}}(i)}, \mathbf{w}_i)'), \quad (8)$$

where $K(\cdot, \cdot)$ is a chosen kernel matrix parameterised by hyperparameters $\mathbf{\Lambda}_i$.

The above approach requires defining a separate model for each causal DAG. Next, we show how to interpret the hyperparameters of this model as an adjacency matrix. This will allow for continuously parameterising the space of graphs.

3.2. Continuous Relaxation: The CGP-CDE Model

The key insight to continuously parameterise graphs in the above model (not DAGs), is that the hyperparameters control dependence between variables (Williams and Rasmussen, 1995). In our Gaussian process prior for a variable X_i , we use kernels with different hyperparameters Λ_{ij} for each dimension j). In general, kernels of this form factorise as $K_{\mathbf{\Lambda}_i}((\mathbf{X}, \mathbf{w}_i), (\mathbf{X}, \mathbf{w}_i)') = K_{\Lambda_{ii}}(\mathbf{w}_i, \mathbf{w}_i') \prod_{j \neq i} K_{\Lambda_{ij}}(\mathbf{x}_j, \mathbf{x}_j')$. Certain hyperparameters of the kernels can then be used to control the variability of the function with respect to specific inputs. We denote these hyperparameters as θ with $\theta \subset \mathbf{\Lambda}$ and all other hyper-

parameters as $\sigma = \Lambda \setminus \theta$. Specifically

$$\theta_{ij} = 0 \implies \frac{\partial f_i}{\partial X_j} = 0.$$

Hence, if the kernel hyperparameter value for θ_{ij} is near zero, the function for variable X_i is constant with respect to variable X_j . Thus we can construct a corresponding adjacency as

$$A_{ij} = \begin{cases} \theta_{ij} & \text{if } j \neq i, \\ 0 & \text{otherwise.} \end{cases} \quad (9)$$

As a value of $\theta_{ij} = 0$ means that changing X_j does not change X_i this corresponds to an absence of an edge from X_j to X_i in \mathbf{A} .

The Gaussian process prior $p(\mathbf{f}_i | \mathbf{X}_{\text{PA}_{\mathcal{G}^{\mathbf{A}}}(i)}, \sigma_i, \theta_i, \mathbf{w}_i)$ is then parameterised as follows

$$\mathcal{N}(\mathbf{0}, K_{\sigma_i, \theta_i}((\mathbf{X}_{-i}, \mathbf{w}_i), (\mathbf{X}_{-i}, \mathbf{w}_i)')), \quad (10)$$

where $\text{PA}_{\mathcal{G}^{\mathbf{A}}}(i)$ denotes the parents of X_i in $\mathcal{G}^{\mathbf{A}}$ (the graph implied by the adjacency \mathbf{A}), and \mathbf{X}_{-i} denotes all variables except X_i . Thus, for a variable X_i , all the other variables are inputs, and the values of the hyperparameters θ_i control the dependence of the rest of the variables \mathbf{X}_{-i} on X_i , and hence define the parents of X_i . The hyperparameters in the above model thus continuously parameterise the space of graphs. The exact kernel we use is in appendix B.1.

3.3. Priors on Graphs

As discussed in Eggeling et al. (2019), not using a prior on graphs leads to a higher weight on denser graphs due to the larger number of dense graphs versus sparse graphs. Hence, to even out this effect, we place a prior that prefers sparser graphs. By introducing priors on the hyperparameters θ in our model, we can effectively encode priors on the graph in eq. (9). We thus place a Gamma prior with parameters chosen to prefer small values of θ , $P(\theta) = \text{Gamma}(\eta, \beta)$. Note that our prior is symmetric between graphs within the same MEC. That is, we do not impose a preference over the causal direction between variables, only over the number of edges in the graph. Other priors on graphs could be considered (Eggeling et al., 2019), but we leave that for future work.

3.4. Score

As stated in section 2.4, our decision rule is to pick the causal graph with the highest posterior probability. For this, we need to calculate the log marginal likelihood for every variable in our model (eq. (3)). To find the log marginal likelihood, we must integrate over the priors of \mathbf{f} and \mathbf{W} , $\log p(\mathbf{x}_i | \mathbf{X}_{\text{PA}_{\mathcal{G}^{\mathbf{A}}}(i)}, \sigma_i, \theta_i, \phi_i)$ is given as

$$\log \int \int p(\mathbf{x}_i | \mathbf{f}_i, \phi_i) p(\mathbf{f}_i | \mathbf{X}_{\text{PA}_{\mathcal{G}^{\mathbf{A}}}(i)}, \mathbf{w}_i, \sigma_i, \theta_i) p(\mathbf{w}_i) d\mathbf{w}_i d\mathbf{f}_i.$$

Calculating this marginal likelihood is analytically intractable due to the non-linear dependence of \mathbf{f}_i on the latent term \mathbf{w}_i . We thus use variational inference, with variational posteriors q , to optimise a tractable lower bound to the marginal likelihood (details and derivation as well as how we handle the rest of the hyperparameters are in appendix B.2). We denote the full lower bound for all variables as $\mathcal{L}_{\text{ELBO}}(q, \theta, \sigma, \phi)$. The optimisation problem is

$$\max_{\theta, \sigma, \phi, q} \mathcal{L}_{\text{ELBO}}(q, \theta, \sigma, \phi) + \log p(\theta) \text{ s.t. } \mathcal{G}^{\mathbf{A}\theta} \in \text{DAGs}.$$

Maximising σ , ϕ , and q gives an accurate estimate of the marginal likelihood while maximising θ finds the graph that maximises the posterior probability.

We can use the function in eq. (5) to convert the condition that $\mathcal{G}^{\mathbf{A}\theta} \in \text{DAGs}$ to $h(\mathbf{A}_\theta) = 0$. The constrained optimisation problem can now be transformed into a sequence of unconstrained optimisation problems, solved using the augmented Lagrange (appendix B.3) (Zheng et al., 2018). The final score is

$$\mathcal{L}_{\text{ELBO}}(q, \theta, \sigma, \phi) + \log p(\theta) - \alpha_t |h(\mathbf{A}_\theta)|^2 - \frac{\rho t}{2} h(\mathbf{A}_\theta). \quad (11)$$

Structure learning has now been converted into a single differentiable optimisation problem.

3.5. Computational Cost

The cost of computing the loss for N samples in a Gaussian Process is usually $\mathcal{O}(N^3)$. We use the uncollapsed inducing point formulation that introduces $M < N$ inducing points allowing for mini-batching (appendix B.2) (Hensman et al., 2013). This changes the cost to $\mathcal{O}(M^3)$. As we have D variables, the total cost is $\mathcal{O}(DM^3)$. The cost of computing the acyclicity regulariser is $\mathcal{O}(D^3)$ for D variables. Hence, the cost is dominated by M or D , whichever is bigger. The choice of the number of inducing points depends on the problem, with more inducing points leading to better approximations (Bauer et al., 2016). However, it is possible to use the lower bound $\mathcal{L}_{\text{ELBO}}$ to find the optimal number of inducing points (Burt et al., 2020). The cost of Gaussian processes, and Bayesian methods in general, can be higher than their non-Bayesian counterparts. Despite this, Bayesian model selection based causal discovery offers other advantages such as the use of more flexible model classes.

4. Related Work

Certain approaches only use information about independences between variables to discover the causal structure, recovering only an MEC, and not the whole DAG (Spirtes et al., 2000; 1995; Chickering, 2002; Huang et al., 2018). Identifying a unique DAG requires additional assumptions,

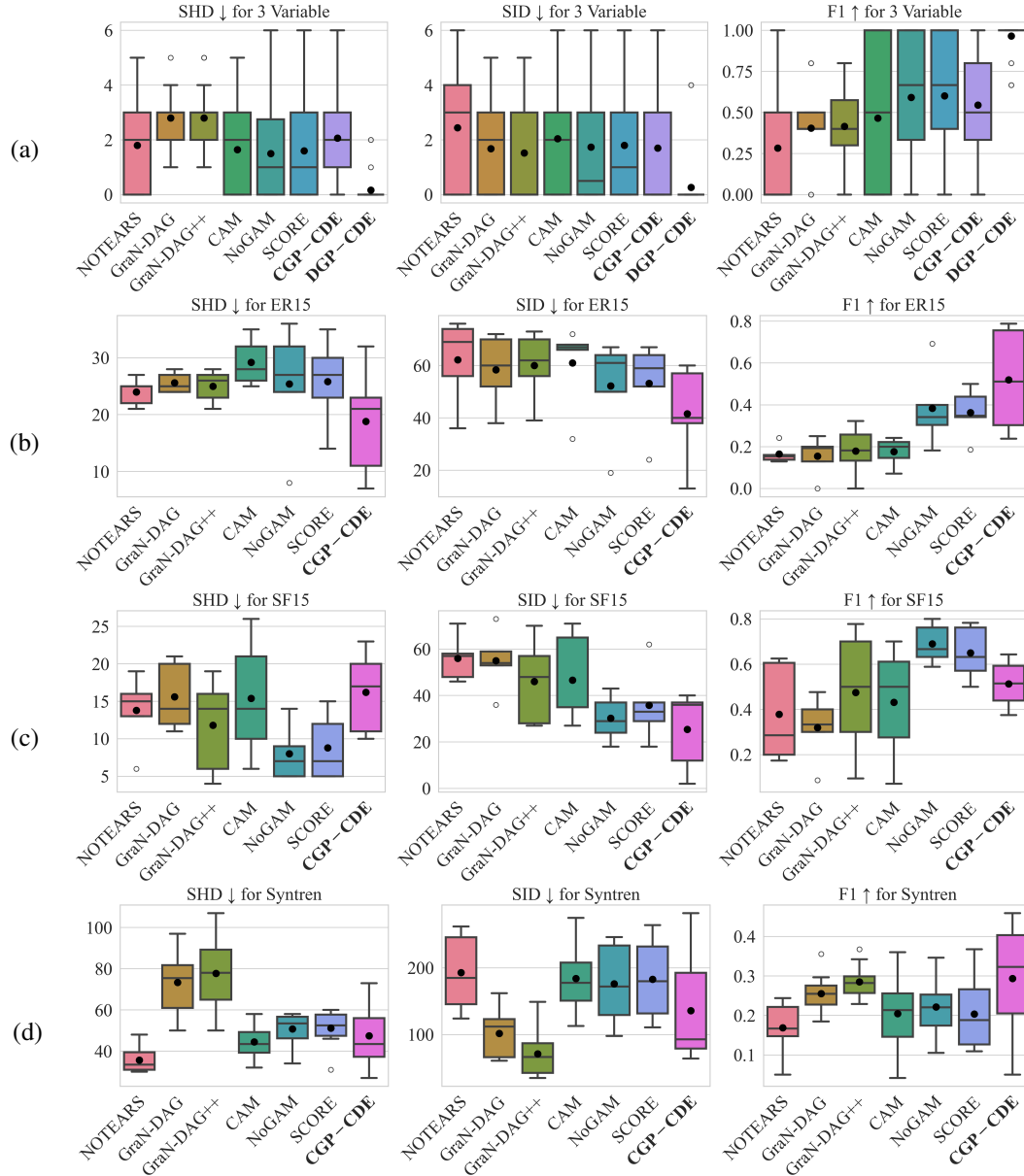


Figure 2. Box plots of metrics for (a) three variable synthetic data (b) Erdos-Renyi (ER) graphs (c) Scale-Free (SF) graphs (d) Syntren data. The plots show the distribution of the metrics across the different datasets for each experiment. The centre line is the median, the black dot is the mean and the white dots represent outliers. Lower is better for SHD and SID, and higher is better for F1.

typically involving restrictions on model classes or access to interventional data (Lippe et al., 2021; Ke et al., 2022; Brouillard et al., 2020; Ke et al., 2020). Since we assume access only to observational data, we focus on the former. Continuous optimisation methods cast causal discovery as a single unconstrained optimisation problem (Zheng et al., 2018). This involves either introducing a regulariser to promote learning DAGs (Zheng et al., 2018; Lachapelle et al., 2019; Yu et al., 2019) or directly parameterising the space of DAGs (Yu et al., 2021; Charpentier et al., 2021). NOTEARS (Zheng et al., 2018) uses a regulariser for learn-

ing linear causal models. Follow-up work, such as GranN-DAG (Lachapelle et al., 2019) and DAG-GNN (Yu et al., 2019), extends this approach to neural networks and graph neural networks. These methods typically restrict models to additive noise (ANM) to recover a DAG, which can limit performance when assumptions are not met (section 2.3).

Other methods first search for node orderings and then prune to ensure a DAG structure. CAM (Bühlmann et al., 2014) uses sparse regression to learn node neighbourhoods and searches for orderings that maximise a score. SCORE (Rol-

land et al., 2022) learns the ordering based on the score function of ANM models with Gaussian noise and then prunes using sparse regression. NOGAM (Montagna et al., 2023) extends SCORE to arbitrary noise distributions. The above methods specifically rely on the ANM assumption.

The Bayesian framework has previously been used for causal discovery, focusing on efficient sampling from the posterior over causal graphs. Geiger and Heckerman (2002) use Bayesian linear Gaussian models but construct their model such that graphs in the same Markov equivalence class receive the same score. Similarly, Cundy et al. (2021) also only consider posteriors over linear Gaussian models. DiBS (Lorch et al., 2021) assumes Bayesian ANMs and parametrises the space of graphs using latent variables. Their method is able to output a fixed number of samples from the posterior over causal graphs. Annadani et al. (2023) also use sampling methods to sample from the posterior over ANM causal models but use a permutation based parametrisation of the graph (Charpentier et al., 2021; Yu et al., 2021).

In contrast, our work uses Bayesian model selection to distinguish causal structures within an MEC that can allow for fewer restrictions than likelihood-based methods (Stegle et al., 2010; Dhir et al., 2024). While previous studies demonstrated this with two variables, we show its feasibility and advantages with multiple variables.

5. Experiments

We compare our approach to various baselines that perform multivariate causal discovery to recover a DAG. We test our method on synthetic data generated from our model (section 5.1), and data not generated from our model (section 5.2). Then we compare our models to the baselines in semi-synthetic and real data cases (section 5.3). See appendix B.6 for full details of the settings used for the CGP-CDE implementation.

It was recently found that causal discovery methods can be sensitive to variance information that is an artefact of synthetic causal datasets or measurement scales in real world datasets (Reisach et al., 2021). Following suggestions in Reisach et al. (2021), we standardise every variable before using our method and the baselines. We note that previous works did not standardise all the datasets, explaining the difference in results from our work (see appendix D).

Baselines: We compare against non-Bayesian counterparts that use similar acyclicity regularisers, such as NOTEARS (Zheng et al., 2018), GraN-DAG, and GraN-DAG++ (Lachapelle et al., 2019), providing a direct comparison of our method’s advantage. NOTEARS assumes linearity, GraN-DAG assumes ANM, and GraN-DAG++ is not identifiable. We also compare against order based methods that first estimate a topological order of the graph

and then prune to get the final graph - SCORE (Rolland et al., 2022), NOGAM (Montagna et al., 2023), and CAM (Bühlmann et al., 2014). These all assume ANM. Details are in appendix F.

Metrics: We use the following metrics to compare the methods. **SHD:** The structural Hamming distance is the Hamming distance between the predicted adjacency and the ground truth adjacency matrix. **SID:** The structural interventional distance counts the number of interventional distributions that are incorrect if the predicted graph is used to form the parent adjustment set instead of the ground truth graph (Peters and Bühlmann, 2015). **F1:** The F1 score is the harmonic mean of the precision and recall, where an edge is considered the positive class.

5.1. Synthetic 3 Variables

Using more flexible estimators may introduce some probability of error (section 2.4, appendix A). First, we answer the question: if the data generating process matches our model, how informative is the MAP value (eq. (1)) about the true causal structure? (appendix A). To estimate the error only due to overlap in posteriors of different causal models, we perform discrete model comparison (labelled DGP-CDE, see appendix C.1 for more details). This involves enumerating and computing the posterior of every causal model. We study the 3 variable case, where it is possible to enumerate every possible causal structure, 25 in total. Here, data is generated from our GP-CDE model, and from each of the 6 distinct causal structures for 3 variables (up to permutations of the variables, details in appendix E). We generate 5 datasets of 1000 samples for each of the graphs leading to 30 datasets in total.

The results for the 3 variable case can be seen in fig. 2 (a). Here, we can see that the discrete comparison DGP-CDE achieves very good performance. This shows that in the GP-CDE model, the overlap between the posteriors of different causal structures is low and that our inference does not contribute greatly to errors. Thus, if the GP-CDE model is a good descriptor of the dataset at hand, we can expect the MAP value to identify the true causal direction with high probability. In Figure 2 (a) the CGP-CDE performs worse across all metrics than the DGP-CDE. This shows that we can expect a higher error due to optimisation of the continuous relaxation in the CGP-CDE.

5.2. Synthetic 10 Variables

Next, we analyse the performance on a higher number of variables. Here, performing discrete model comparison is too costly as the number of DAGs is prohibitively large, so we use our continuous relaxation, labelled CGP-CDE. We generate 10 node graphs using Erdos-Renyi (ER) and scale-free (SF) (Barabási and Albert, 1999) schemes with

15 expected edges. In ER graphs, each edge is generated independently while SF graphs promote a few nodes with a high number of edges. The data is generated from randomly initialised neural networks with noise included as an input. This ensures that the data is not sampled from any of the baselines or the CGP-CDE model. Performing well in such cases showcases the advantage of the added flexibility in the Bayesian approach. Data generation details are in appendix E.

The results for the 10 variable synthetic datasets can be seen in fig. 2 (b) and (c). Compared to the DGP-CDE results of section 5.1, we can expect a higher number of errors due to the continuous relaxation, as well as the shift in the data generation process. Nevertheless, for the ER graph, the CGP-CDE method outperforms the baselines in terms of the mean SHD, SID and F1 scores. For the SF graphs, CGP-CDE performs competitively, achieving better mean SID and F1 scores for most methods except for NOGAM and SCORE. In the SF graphs, a few variables cause the rest of the variables. We hypothesise that this structure benefits the topological search that NOGAM and SCORE perform.

5.3. Syntren and Sachs

Table 1. Results for Sachs dataset (Sachs et al., 2005). Lower is better for SHD, SID, higher is better for F1.

Method	SHD ↓	SID ↓	F1 ↑
NOTEARS	14	49	0.36
GraN-DAG	19	57	0.30
GraN-DAG ++	18	55	0.31
CAM	18	56	0.36
SCORE	23	59	0.15
NOGAM	23	59	0.15
CGP-CDE	17	59	0.48

Syntren is a semi-synthetic dataset that takes real biological graphs and generates datasets according to a simulator. There are 10 datasets of 20 nodes with 500 samples each. The Sachs dataset (Sachs et al., 2005) is a real dataset that measures the expression levels of proteins. It contains 853 observational samples and 11 nodes. Details for both are in appendix E.

The results on Syntren can be seen in fig. 2 (d). Here, the CGP-CDE performs competitively in terms of F1 and SHD scores, only losing out to GraN-DAG and GraN-DAG++ in SID. However, GraN-DAG and GraN-DAG++ perform worse in terms of SHD and F1. The SID score does not penalise extra edges. Syntren has on average 23.5 edges. While CGP-CDE predicts 45.4, GraN-DAG and GraN-DAG++ predict 79.7 and 74.8 respectively. The results for Sachs can be seen in table 1. The CGP-CDE outperforms all the methods here in terms F1 scores. NOTEARS

performs well on SHD and SID but only predicts 4 edges, whereas CGP-CDE predicts 15. The ground truth has 18 edges.

6. Conclusion

We have introduced a continuous relaxation approach to Bayesian model selection for multivariate causal discovery. This method casts the problem as a single differentiable optimisation task, allowing the use of more flexible models compared to traditional methods. Our approach demonstrates competitive performance across various synthetic and real-world datasets, highlighting its versatility. By allowing scalable causal discovery without restrictive assumptions, we illustrate that Bayesian model selection is effective and could allow for more practical causal discovery.

References

- Yashas Annadani, Nick Pawlowski, Joel Jennings, Stefan Bauer, Cheng Zhang, and Wenbo Gong. BayesDAG: Gradient-based posterior inference for causal discovery. In *Thirty-seventh Conference on Neural Information Processing Systems*, 2023. URL <https://openreview.net/forum?id=woptnU6fh1>. [Cited on page 7.]
- Albert-László Barabási and Réka Albert. Emergence of scaling in random networks. *science*, 286(5439), 1999. [Cited on pages 7 and 19.]
- Matthias Bauer, Mark Van der Wilk, and Carl Edward Rasmussen. Understanding probabilistic sparse gaussian process approximations. *Advances in neural information processing systems*, 29, 2016. [Cited on page 5.]
- Philippe Brouillard, Sébastien Lachapelle, Alexandre Lacoste, Simon Lacoste-Julien, and Alexandre Drouin. Differentiable causal discovery from interventional data. *Advances in Neural Information Processing Systems*, 33, 2020. [Cited on page 6.]
- Peter Bühlmann, Jonas Peters, and Jan Ernest. Cam: Causal additive models, high-dimensional order search and penalized regression. *The Annals of Statistics*, 42(6), 2014. [Cited on pages 6, 7, 19, and 20.]
- David R Burt, Carl Edward Rasmussen, and Mark Van Der Wilk. Convergence of sparse variational inference in gaussian processes regression. *Journal of Machine Learning Research*, 21(131), 2020. [Cited on page 5.]
- Bertrand Charpentier, Simon Kibler, and Stephan Günnemann. Differentiable dag sampling. In *International Conference on Learning Representations*, 2021. [Cited on pages 6 and 7.]

- David Maxwell Chickering. Optimal structure identification with greedy search. *Journal of machine learning research*, 3(Nov), 2002. [Cited on page 5.]
- Chris Cundy, Aditya Grover, and Stefano Ermon. Bcd nets: Scalable variational approaches for bayesian causal discovery. *Advances in Neural Information Processing Systems*, 34, 2021. [Cited on page 7.]
- Anish Dhir, Samuel Power, and Mark Van Der Wilk. Bivariate causal discovery using Bayesian model selection. In *Proceedings of the 41st International Conference on Machine Learning*, volume 235 of *Proceedings of Machine Learning Research*. PMLR, 2024. [Cited on pages 1, 2, 3, 7, 12, and 16.]
- Vincent Dutoridoir, Hugh Salimbeni, James Hensman, and Marc Deisenroth. Gaussian process conditional density estimation. *Advances in neural information processing systems*, 31, 2018. [Cited on pages 4, 12, 13, 14, and 15.]
- Ralf Eggeling, Jussi Viinikka, Aleksis Vuoksenmaa, and Mikko Koivisto. On structure priors for learning bayesian networks. In *The 22nd International Conference on Artificial Intelligence and Statistics*. PMLR, 2019. [Cited on page 5.]
- Paul Erdos, Alfréd Rényi, et al. On the evolution of random graphs. *Publ. math. inst. hung. acad. sci.*, 5(1):17–60, 1960. [Cited on page 19.]
- Stefan Feuerriegel, Dennis Frauen, Valentyn Melnychuk, Jonas Schweisthal, Konstantin Hess, Alicia Curth, Stefan Bauer, Niki Kilbertus, Isaac S Kohane, and Mihaela van der Schaar. Causal machine learning for predicting treatment outcomes. *Nature Medicine*, 30(4):958–968, 2024. [Cited on page 1.]
- Nir Friedman and Iftach Nachman. Gaussian process networks. In *Proceedings of the Sixteenth conference on Uncertainty in artificial intelligence*, 2000. [Cited on page 3.]
- Dan Geiger and David Heckerman. Parameter priors for directed acyclic graphical models and the characterization of several probability distributions. *The Annals of Statistics*, 30(5), 2002. [Cited on pages 2, 3, and 7.]
- Isabelle Guyon, Olivier Goudet, and Diviyam Kalainathan. Evaluation methods of cause-effect pairs. In *Cause Effect Pairs in Machine Learning*, chapter 2. Springer, 2019. [Cited on pages 3 and 12.]
- Kaiming He, Xiangyu Zhang, Shaoqing Ren, and Jian Sun. Delving deep into rectifiers: Surpassing human-level performance on imagenet classification. In *Proceedings of the IEEE international conference on computer vision*, 2015. [Cited on page 17.]
- David Heckerman. A bayesian approach to learning causal networks. In *Proceedings of the Eleventh conference on Uncertainty in artificial intelligence*, pages 285–295, 1995. [Cited on page 3.]
- David Heckerman and Dan Geiger. Likelihoods and parameter priors for bayesian networks. 1995. [Cited on page 3.]
- David Heckerman, Dan Geiger, and David M Chickering. Learning bayesian networks: The combination of knowledge and statistical data. *Machine learning*, 20(3), 1995. [Cited on page 3.]
- James Hensman, Nicolo Fusi, and Neil D Lawrence. Gaussian processes for big data. *arXiv preprint arXiv:1309.6835*, 2013. [Cited on pages 5, 12, 15, 17, and 18.]
- John Hicks et al. *Causality in economics*. Australian National University Press, 1980. [Cited on page 1.]
- Patrik Hoyer, Dominik Janzing, Joris M Mooij, Jonas Peters, and Bernhard Schölkopf. Nonlinear causal discovery with additive noise models. *Advances in neural information processing systems*, 21, 2008. [Cited on pages 1 and 3.]
- Biwei Huang, Kun Zhang, Yizhu Lin, Bernhard Schölkopf, and Clark Glymour. Generalized score functions for causal discovery. In *Proceedings of the 24th ACM SIGKDD international conference on knowledge discovery & data mining*, 2018. [Cited on page 5.]
- Alexander Immer, Christoph Schultheiss, Julia E Vogt, Bernhard Schölkopf, Peter Bühlmann, and Alexander Marx. On the identifiability and estimation of causal location-scale noise models. In *International Conference on Machine Learning*. PMLR, 2023. [Cited on page 12.]
- Dominik Janzing and Bernhard Schölkopf. Causal inference using the algorithmic markov condition. *IEEE Transactions on Information Theory*, 56(10), 2010. [Cited on page 2.]
- Robert E Kass and Adrian E Raftery. Bayes factors. *Journal of the american statistical association*, 90(430), 1995. [Cited on page 3.]
- Nan Rosemary Ke, Olexa Bilaniuk, Anirudh Goyal, Stefan Bauer, Hugo Larochelle, Bernhard Schölkopf, Michael C Mozer, Chris Pal, and Yoshua Bengio. Learning neural causal models from unknown interventions. *stat*, 1050: 23, 2020. [Cited on page 6.]
- Nan Rosemary Ke, Silvia Chiappa, Jane X Wang, Jorg Bornschein, Anirudh Goyal, Melanie Rey, Theophane Weber, Matthew Botvinick, Michael Curtis Mozer, and

- Daniilo Jimenez Rezende. Learning to induce causal structure. In *International Conference on Learning Representations*, 2022. [Cited on page 6.]
- Diederik P Kingma and Jimmy Ba. Adam: A method for stochastic optimization. *arXiv preprint arXiv:1412.6980*, 2014. [Cited on pages 17 and 18.]
- Sébastien Lachapelle, Philippe Brouillard, Tristan Deleu, and Simon Lacoste-Julien. Gradient-based neural dag learning. In *International Conference on Learning Representations*, 2019. [Cited on pages 6, 7, 15, 16, 19, and 20.]
- Vidhi Lalchand, Aditya Ravuri, and Neil D Lawrence. Generalised gaussian process latent variable models (gplvm) with stochastic variational inference. *arXiv preprint arXiv:2202.12979*, 2022. [Cited on pages 2, 13, and 15.]
- Haichao Li, Kun Wu, Chenchen Ruan, Jiao Pan, Yujin Wang, and Hongan Long. Cost-reduction strategies in massive genomics experiments. *Marine Life Science & Technology*, 1, 2019. [Cited on page 1.]
- Phillip Lippe, Taco Cohen, and Efstratios Gavves. Efficient neural causal discovery without acyclicity constraints. In *International Conference on Learning Representations*, 2021. [Cited on page 6.]
- Lars Lorch, Jonas Rothfuss, Bernhard Schölkopf, and Andreas Krause. Dibs: Differentiable bayesian structure learning. *Advances in Neural Information Processing Systems*, 34, 2021. [Cited on page 7.]
- David JC MacKay. Comparison of approximate methods for handling hyperparameters. *Neural computation*, 11(5), 1999. [Cited on page 15.]
- Francesco Montagna, Nicoletta Noceti, Lorenzo Rosasco, Kun Zhang, and Francesco Locatello. Causal discovery with score matching on additive models with arbitrary noise. In *Conference on Causal Learning and Reasoning*. PMLR, 2023. [Cited on pages 7 and 19.]
- Joris M Mooij, Jonas Peters, Dominik Janzing, Jakob Zscheischler, and Bernhard Schölkopf. Distinguishing cause from effect using observational data: methods and benchmarks. *The Journal of Machine Learning Research*, 17(1), 2016. [Cited on page 19.]
- AS Nemirovsky. Optimization ii. numerical methods for nonlinear continuous optimization. 1999. [Cited on pages 4 and 15.]
- Judea Pearl. *Causality*. Cambridge university press, 2009. [Cited on pages 2, 3, and 12.]
- Jonas Peters and Peter Bühlmann. Structural intervention distance for evaluating causal graphs. *Neural computation*, 27(3), 2015. [Cited on page 7.]
- Jonas Peters, Dominik Janzing, and Bernhard Schölkopf. *Elements of causal inference: foundations and learning algorithms*. The MIT Press, 2017. [Cited on pages 1 and 2.]
- Carl Edward Rasmussen. Gaussian processes in machine learning. In *Summer school on machine learning*. Springer, 2003. [Cited on pages 4, 12, 15, and 16.]
- Alexander Reisach, Christof Seiler, and Sebastian Weichwald. Beware of the simulated dag! causal discovery benchmarks may be easy to game. *Advances in Neural Information Processing Systems*, 34, 2021. [Cited on pages 7 and 18.]
- Paul Rolland, Volkan Cevher, Matthäus Kleindessner, Chris Russell, Dominik Janzing, Bernhard Schölkopf, and Francesco Locatello. Score matching enables causal discovery of nonlinear additive noise models. In *International Conference on Machine Learning*. PMLR, 2022. [Cited on pages 6, 7, and 19.]
- Karen Sachs, Omar Perez, Dana Pe’er, Douglas A Lauffenburger, and Garry P Nolan. Causal protein-signaling networks derived from multiparameter single-cell data. *Science*, 308(5721), 2005. [Cited on pages 1, 2, 8, and 19.]
- Hugh Salimbeni, Stefanos Eleftheriadis, and James Hensman. Natural gradients in practice: Non-conjugate variational inference in gaussian process models. In *International Conference on Artificial Intelligence and Statistics*. PMLR, 2018. [Cited on page 17.]
- Peter Spirtes, Christopher Meek, and Thomas Richardson. Causal inference in the presence of latent variables and selection bias. In *Proceedings of the Eleventh conference on Uncertainty in artificial intelligence*, 1995. [Cited on page 5.]
- Peter Spirtes, Clark N Glymour, and Richard Scheines. *Causation, prediction, and search*. 2000. [Cited on page 5.]
- Oliver Stegle, Dominik Janzing, Kun Zhang, Joris M Mooij, and Bernhard Schölkopf. Probabilistic latent variable models for distinguishing between cause and effect. *Advances in neural information processing systems*, 23, 2010. [Cited on pages 3 and 7.]
- Michalis Titsias. Variational learning of inducing variables in sparse gaussian processes. In *Artificial intelligence and statistics*. PMLR, 2009. [Cited on pages 14, 15, and 17.]

- Michalis Titsias and Neil D Lawrence. Bayesian gaussian process latent variable model. In *Proceedings of the thirteenth international conference on artificial intelligence and statistics*. JMLR Workshop and Conference Proceedings, 2010. [Cited on pages 2, 12, 14, and 15.]
- Tim Van den Bulcke, Koenraad Van Leemput, Bart Naudts, Piet van Remortel, Hongwu Ma, Alain Verschoren, Bart De Moor, and Kathleen Marchal. Syntren: a generator of synthetic gene expression data for design and analysis of structure learning algorithms. *BMC bioinformatics*, 7, 2006. [Cited on page 19.]
- Christopher Williams and Carl Rasmussen. Gaussian processes for regression. *Advances in neural information processing systems*, 8, 1995. [Cited on page 4.]
- Christopher K Williams and Carl Edward Rasmussen. *Gaussian processes for machine learning*, volume 2. MIT press Cambridge, MA, 2006. [Cited on page 13.]
- Yue Yu, Jie Chen, Tian Gao, and Mo Yu. Dag-gnn: Dag structure learning with graph neural networks. In *International Conference on Machine Learning*. PMLR, 2019. [Cited on pages 6, 15, and 19.]
- Yue Yu, Tian Gao, Naiyu Yin, and Qiang Ji. Dags with no curl: An efficient dag structure learning approach. In *International Conference on Machine Learning*. Pmlr, 2021. [Cited on pages 6 and 7.]
- Kun Zhang and Aapo Hyvarinen. On the identifiability of the post-nonlinear causal model. *arXiv preprint arXiv:1205.2599*, 2012. [Cited on page 12.]
- Kun Zhang, Zhikun Wang, Jiji Zhang, and Bernhard Schölkopf. On estimation of functional causal models: general results and application to the post-nonlinear causal model. *ACM Transactions on Intelligent Systems and Technology (TIST)*, 7(2), 2015. [Cited on pages 3 and 12.]
- Xun Zheng, Bryon Aragam, Pradeep K Ravikumar, and Eric P Xing. Dags with no tears: Continuous optimization for structure learning. *Advances in Neural Information Processing Systems*, 31, 2018. [Cited on pages 1, 4, 5, 6, 7, 15, 19, and 20.]

A. Discussion on Identifiability and Probability of Error

With only observational data it is possible to recover the Markov equivalence class (MEC) of a causal structure with only the Markov and faithfulness assumptions (Pearl, 2009). To recover a DAG within an MEC, additional assumptions are required. Here we provide background on the assumptions that provide strict identifiability and the Bayesian model selection approach that allows for more flexible model classes but may incur some probability of error.

The probability of error can be defined as the error made by a model and a decision rule when multiple datasets are sampled from the model itself (Guyon et al., 2019; Dhir et al., 2024). Restrictive assumptions on models such as additive-noise (ANM), provide a strict notion of identifiability with maximum likelihood (Zhang et al., 2015), where the probability of error is 0 (fig. 3 (b)). This suggests, that if the data is sampled from an ANM, the causal direction can be recovered with probability 1 (in the population setting). Other examples of restricted model classes include post non-linear noise models (PNL) (Zhang and Hyvarinen, 2012), and location-scale noise models (Immer et al., 2023). However, if the data generating process deviates from these restrictions, then the above guarantee no longer holds.

Bayesian model selection preserves the guarantees of maximum likelihood based approaches if suitably restricted model classes are used (Dhir et al., 2024, Prop. 4.5). However, for more flexible model classes, maximum likelihood based approaches are completely non-informative within a Markov equivalence class (fig. 3(a)) (Zhang et al., 2015, Lemma 1). For these flexible model classes, Bayesian model selection can still be informative (Dhir et al., 2024, Prop. 4.7). Bayesian model selection involves placing priors on a model’s functions or parameters, thereby assigning priors over its distributions. These priors are constructed to encode the Independent Causal Mechanisms (ICM) assumption in a specific causal direction; changing the causal direction alters how the ICM assumption is applied. The marginal likelihood then estimates the probability that the observed data were generated under the model’s prior and corresponding ICM assumption. Because the marginal likelihood must sum to one over all possible datasets (see fig. 3 (c)), it cannot assign equal probability to different causal directions under the same prior and its ICM assumption (unless under certain conditions hold (Dhir et al., 2024, Corollary. 4.8)). Here, the probability of error may no longer be 0 as the posteriors may overlap (fig. 3(c)). The advantage of the Bayesian approach is that the more flexible assumptions may mitigate misspecification in cases where more flexibility is required to model the data well and the guarantees of restricted models do not hold anyway. This probability of error can be estimated by sampling datasets from the model and classifying the causal direction (Dhir et al., 2024, Sec. 4.3). We perform this in section 5.1.

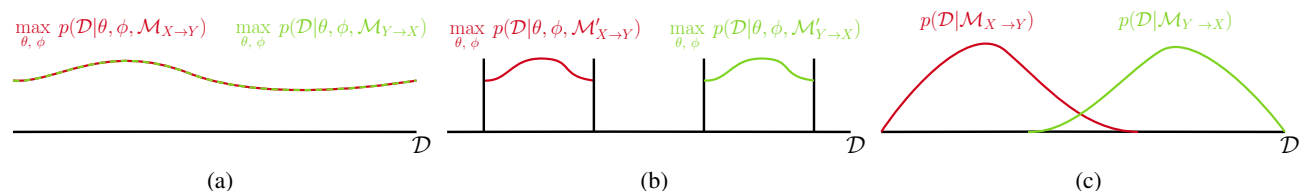


Figure 3. Reproduced from Dhir et al. (2024) with permission from authors. (a) Maximum likelihood based methods cannot distinguish causal models that are within a Markov Equivalence Class. (b) Making suitable restrictions allows for maximum likelihood to identify the causal direction, but restricts the datasets that can be modelled. (c) Bayesian model selection relaxes these restrictions by incorporating priors that encode the Independent Causal Mechanisms (ICM) assumption. This approach offers greater modelling flexibility and enables estimation of how likely it is that a dataset was generated under the prior and encoded ICM assumption.

B. CGP-CDE Details

For our Bayesian causal model, we use the Gaussian process conditional density estimator (Dutordoir et al., 2018). We use a sum of commonly used kernels (Rasmussen, 2003, Ch. 5), as outlined in appendix B.1. We also apply variational inference to optimise the lower bound, as is standard for latent variable Gaussian process models (Dutordoir et al., 2018; Titsias and Lawrence, 2010) and use inducing points with stochastic variational inference to improve data scalability (Hensman et al., 2013). We outline the variational inference in appendix B.2 and detail our optimisation schedule in appendix B.3.

B.1. CGP-CDE Kernel

The ultimate aim of the approach is to find the causal graph that maximises the posterior probability. The choice of kernels will be problem dependent and it is possible to carry out Bayesian model selection over the kernels themselves (Rasmussen,

2003, Ch. 5). To allow for good fits of a range of datasets, we use a sum of kernels that can express functions with a range of lengthscales and roughness well.

The kernel for function f_i is

$$k_i = k_{\text{lin},i} + k_{\text{sqe},i} + k_{\text{m12},i} + k_{\text{m32},i} + k_{\text{rq},i}, \quad (12)$$

where each of the kernels is defined below (Williams and Rasmussen, 2006, Ch. 4). For all the kernels, θ_{ii} is the hyperparameter for the latent dimension.

$k_{\text{lin},i}$ is the linear kernel:

$$k_{\text{lin},i} = \sum_{j \neq i}^D \theta_{\text{lin},ij} x_j x'_j + \theta_{\text{lin},ii} w_i w'_i, \quad (13)$$

where $\theta_{\text{lin},ij}$ indicates the j^{th} dimension of hyperparameter $\theta_{\text{lin},i}$.

$k_{\text{sqe},i}$ is the squared exponential kernel

$$k_{\text{sqe},i} = \sigma_{\text{sqe},i}^2 \left(\sum_{j \neq i}^D \exp \left(-\theta_{\text{sqe},ij}^2 \frac{(x_j - x'_j)^2}{2} \right) + \exp \left(-\theta_{\text{sqe},ii}^2 \frac{(w_i - w'_i)^2}{2} \right) \right), \quad (14)$$

where θ_{sqe} is the precision parameter.

$k_{\text{m12},i}$ and $k_{\text{m32},i}$ are the Matérn12 and Matérn32 kernels with $\nu = \frac{1}{2}$ and $\nu = \frac{3}{2}$ respectively, with the general form

$$k_{\text{m}\nu,i} = \sigma_{\text{m}\nu,i}^2 \sum_{j \neq i}^D \frac{2^{1-\nu}}{\Gamma(\nu)} \left(\theta_{\text{m}\nu,ij} \sqrt{2\nu} |x_j - x'_j| \right)^\nu K_\nu \left(\theta_{\text{m}\nu,ij} \sqrt{2\nu} |x_j - x'_j| \right) \\ + \sigma_{\text{m}\nu,i}^2 \frac{2^{1-\nu}}{\Gamma(\nu)} \left(\theta_{\text{m}\nu,ii} \sqrt{2\nu} |w_i - w'_i| \right)^\nu B_\nu \left(\theta_{\text{m}\nu,ii} \sqrt{2\nu} |w_i - w'_i| \right), \quad (15)$$

where $\Gamma(\nu)$ is the gamma functions and B_ν is a modified Bessel function. Similarly to the squared exponential kernel, $\theta_{\text{m}\nu}$ is the precision parameter.

$k_{\text{rq},i}$ is the rational quadratic kernel, which is equivalent to the sum of many squared exponential kernels with different precision hyperparameters (Williams and Rasmussen, 2006, Ch. 4),

$$k_{\text{rq},i} = \sigma_{\text{rq},i}^2 \left(\sum_{j \neq i}^D \left(1 + \theta_{\text{rq},ij}^2 \frac{(x_j - x'_j)^2}{2a_d} \right)^{-a_i} + \left(1 + \theta_{\text{rq},ii}^2 \frac{(w_i - w'_i)^2}{2a_i} \right)^{-a_i} \right), \quad (16)$$

where a is a hyperparameter that is learned.

The kernel variance terms σ_{sqe}^2 , $\sigma_{\text{m}\nu}^2$ and σ_{rq}^2 mean individual kernels can be ‘‘switched off’’ by setting this term to zero if they do not contribute to improving the evidence lower bound.

In all these kernels, the hyperparameter denoted by θ controls the variability of the function, as discussed in subsection 3.2. This means as they tend to zero, the input and output of the function become decorrelated. To construct the adjacency matrix in Equation 9, we sum these hyperparameters, so that

$$\theta_{ij} = \theta_{\text{lin},ij} + \theta_{\text{sqe},ij} + \theta_{\text{m12},ij} + \theta_{\text{m32},ij} + \theta_{\text{rq},ij}. \quad (17)$$

B.2. CGP-CDE Lower Bound

We use a variant on the GP-CDE (Dutordoir et al., 2018) to define our causal model and define a prior over distributions. Intractability in these models is commonly solved using variational inference (Lalchand et al., 2022; Dutordoir et al., 2018).

Each variable \mathbf{x}_i is modelled as a function of all other variables \mathbf{X}_{-i} and latent variable \mathbf{w}_d plus some Gaussian noise, parameterised by noise variance ϕ_i^2 :

$$\mathbf{x}_i = \mathbf{f}_i(\mathbf{X}_{-i}, \mathbf{w}_i) + \varepsilon, \quad \varepsilon \sim \mathcal{N}(0, \phi_i^2). \quad (18)$$

The presence of the latent variable allows learning of non-Gaussian and heteroscedastic noise (Dutordoir et al., 2018). A Gaussian process prior is placed on \mathbf{f}_i ,

$$p(\mathbf{f}_i | \mathbf{X}_{\text{PA}_{\mathcal{G}\mathbf{A}}(i)}, \mathbf{\Lambda}_i, \mathbf{w}_i) = \mathcal{N}(\mathbf{0}, K_{\mathbf{\Lambda}_i}((\mathbf{X}_{-i}, \mathbf{w}_i), (\mathbf{X}_{-i}, \mathbf{w}_i)')), \quad (19)$$

where $\mathbf{X}_{\text{PA}_{\mathcal{G}\mathbf{A}}(i)}$ are the parents of \mathbf{x}_i in \mathbf{A} , and K is the kernel with set of hyperparameters denoted $\mathbf{\Lambda}_i$. We denote kernel hyperparameters that control dependence and are included in the adjacency matrix collectively as $\boldsymbol{\theta}$, while the rest as $\boldsymbol{\sigma}$, with $\mathbf{\Lambda} = \{\boldsymbol{\theta}, \boldsymbol{\sigma}\}$.

Different prior beliefs of the form of f can be expressed in the choice of kernel. To find the causal DAG with the highest posterior, we need to maximise the marginal likelihood of each variable. This is written as

$$\log p(\mathbf{x}_i | \mathbf{X}_{\text{PA}_{\mathcal{G}\mathbf{A}}(i)}, \mathbf{\Lambda}_i, \phi_i) = \log \int \int p(\mathbf{x}_i | \mathbf{f}_i, \phi_i) p(\mathbf{f}_i | \mathbf{X}_{\text{PA}_{\mathcal{G}\mathbf{A}}(i)}, \mathbf{\Lambda}_i, \mathbf{w}_i) p(\mathbf{w}_i) d\mathbf{w}_i d\mathbf{f}_i.$$

However, the latent variables \mathbf{w}_i appear non-linearly in $p(\mathbf{f}_i | \mathbf{X}_{\text{PA}_{\mathcal{G}\mathbf{A}}(i)}, \mathbf{\Lambda}_i, \mathbf{w}_i)$ making the calculation of $\log p(\mathbf{x}_i | \mathbf{X}_{\text{PA}_{\mathcal{G}\mathbf{A}}(i)}, \mathbf{\Lambda}_i, \phi_i)$ analytically intractable.

The addition of inducing points \mathbf{u}_i , with corresponding inducing inputs \mathbf{Z}_i , helps both with the intractability of $\log p(\mathbf{x}_i | \mathbf{X}_{\text{PA}_{\mathcal{G}\mathbf{A}}(i)}, \mathbf{\Lambda}_i, \phi_i)$ and scaling to large datasets (Titsias, 2009; Titsias and Lawrence, 2010). We can write the joint between \mathbf{f} and \mathbf{u}_i as:

$$p\left(\begin{bmatrix} \mathbf{f}_i \\ \mathbf{u}_i \end{bmatrix}\right) = \mathcal{N}\left(\begin{bmatrix} \mathbf{0} \\ \mathbf{0} \end{bmatrix}, \begin{bmatrix} K_{i,\mathbf{ff}} & K_{i,\mathbf{fu}} \\ K_{i,\mathbf{uf}} & K_{i,\mathbf{uu}} \end{bmatrix}\right), \quad (20)$$

where $K_{\mathbf{ff}}$ is the covariance matrix between training data, $K_{\mathbf{uu}}$ is the covariance matrix between inducing points and $K_{\mathbf{fu}}$ and $K_{\mathbf{uf}}$ are the covariance matrices between the two. Suppressing the hyperparameters and \mathbf{Z}_i for brevity, the marginal likelihood can then be written as:

$$\log p(\mathbf{x}_i | \mathbf{X}_{\text{PA}_{\mathcal{G}\mathbf{A}}(i)}) = \log \int \int p(\mathbf{x}_i | \mathbf{f}_i) p(\mathbf{f}_i | \mathbf{X}_{\text{PA}_{\mathcal{G}\mathbf{A}}(i)}, \mathbf{w}_i, \mathbf{u}_i) p(\mathbf{w}_i) p(\mathbf{u}_i) d\mathbf{w}_i d\mathbf{f}_i d\mathbf{u}_i. \quad (21)$$

where $p(\mathbf{u}_i) = \mathcal{N}(\mathbf{0}, K_{i,\mathbf{uu}})$. This is still not tractable, so we use variational inference to define an evidence lower bound (ELBO) to the marginal likelihood (Titsias, 2009). This is done by introducing a variational distribution $q(\mathbf{f}_i, \mathbf{w}_i, \mathbf{u}_i)$ and rewriting the marginal likelihood as (suppressing conditioning terms for neatness):

$$\log p(\mathbf{x}_i) = \log \int \int \int p(\mathbf{x}_i | \mathbf{f}_i, \phi_i) p(\mathbf{f}_i | \mathbf{u}_i, \mathbf{X}_{\text{PA}_{\mathcal{G}\mathbf{A}}(i)}, \mathbf{w}_i) p(\mathbf{u}_i) p(\mathbf{w}_i) \frac{q(\mathbf{f}_i, \mathbf{w}_i, \mathbf{u}_i)}{q(\mathbf{f}_i, \mathbf{w}_i, \mathbf{u}_i)} d\mathbf{u}_i d\mathbf{w}_i d\mathbf{f}_i,$$

The variational distribution takes the form (Titsias and Lawrence, 2010; Dutordoir et al., 2018):

$$q(\mathbf{f}_i, \mathbf{w}_i, \mathbf{u}_i) = p(\mathbf{f}_i | \mathbf{w}_i, \mathbf{u}_i) q(\mathbf{w}_i) q(\mathbf{u}_i), \quad (22)$$

where $q(\mathbf{u}_i) = \mathbf{N}(\mathbf{u}_i | \mathbf{m}_{u,i}, \mathbf{S}_{u,i})$ is the Gaussian variational distribution of inducing points \mathbf{u}_i and $q(\mathbf{w}_i) = \mathcal{N}(\boldsymbol{\mu}_i, \boldsymbol{\Sigma}_i)$ is the variational distribution of \mathbf{w}_i .

Rearranging and using Jensen's inequality, we can then get the lower bound for variable d as (Dutordoir et al., 2018)

$$\log p(\mathbf{x}_i) \geq \left\langle \langle \log p(\mathbf{x}_i | \mathbf{f}_i) \rangle_{q(\mathbf{f}_i)} \right\rangle_{q(\mathbf{w}_i)} - KL[q(\mathbf{u}) || p(\mathbf{u})] - KL[q(\mathbf{w}_i) || p(\mathbf{w}_i)], \quad (23)$$

where $q(\mathbf{f}_i) = \int p(\mathbf{f}_i|\mathbf{u}, \mathbf{w}_i)q(\mathbf{u})d\mathbf{u}$. We denote the lower bound for variable X_i as $\mathcal{F}_i(q_i, \mathbf{\Lambda}_i, \phi_i)$. The full lower bound then is $\mathcal{L}_{\text{ELBO}}(q, \mathbf{\Lambda}_i, \phi_i) := \sum_{i=1}^D \mathcal{F}_i(q_i, \mathbf{\Lambda}_i, \phi_i)$, remembering $\mathbf{\Lambda} = \{\boldsymbol{\theta}_i, \boldsymbol{\sigma}_i\}$.

By incorporating the optimal Gaussian variational distribution $q(\mathbf{u})$, which can be calculated in closed form, it is possible to collapse the bound by integrating out the inducing variables (Titsias, 2009; Titsias and Lawrence, 2010). However, the computational complexity of this approach is $\mathcal{O}(NM^2D)$, meaning for large values of N training becomes infeasible (Lalchand et al., 2022). To allow our method to scale to large datasets, we follow the approach of Hensman et al. (2013) and keep $q(\mathbf{u})$ uncollapsed so that stochastic variational inference can be used. This means the data can be minibatched in training, reducing the computational complexity to $\mathcal{O}(M^3D)$. To further improve computational efficiency, we use an encoder to learn a function $h_{q,i} : (\mathbf{x}_{\text{batch}}) \mapsto (\mu_i, \Sigma_i)$ for the variational distribution $q(\mathbf{w}_i) = \mathcal{N}(\mu_i, \Sigma_i)$, where $\mathbf{x}_{\text{batch}} \in \mathbb{R}^{b \times D}$ is a batch of data points, $\mu_i \in \mathbb{R}^b$ and $\Sigma_i \in \mathbb{R}^b$ for batch size b (Dutordoir et al., 2018). This is more efficient than the alternative of learning N parameters. We use a multi-layer perceptron for the encoder and list the hyperparameters used in table 2.

Table 2. Hyperparameters for the variational encoder $h_{q,i} : (\mathbf{x}_{\text{batch}}) \mapsto (\mu_i, \Sigma_i)$.

Parameter	Value
hidden layer size	128
number of layers	5
activation function	ReLU

Other hyperparameters: We follow common practice and maximise the lower bound with respect to the hyperparameters $\boldsymbol{\sigma}$ and ϕ as well (Rasmussen, 2003) (along with $\boldsymbol{\theta}$ and q). This is justified based on the fact that the posterior for these hyperparameters tends to be highly peaked in practice (MacKay, 1999). Thus, a Laplace approximation can be approximated by the maximum value.

B.3. Optimisation schedule

The final score, optimised using the augmented Lagrange method (Zheng et al., 2018; Lachapelle et al., 2019), is

$$\mathcal{L}_{\text{ELBO}}(q, \boldsymbol{\theta}, \boldsymbol{\sigma}, \phi) := \mathcal{L}_{\text{ELBO}}(q, \boldsymbol{\theta}, \boldsymbol{\sigma}, \phi) + \log p(\boldsymbol{\theta}) - \alpha_t |h(\mathbf{A}_{\boldsymbol{\theta}})|^2 - \frac{\rho_t}{2} h(\mathbf{A}_{\boldsymbol{\theta}}), \quad (24)$$

where t is the index of the subproblem and α_t, ρ_t are hyperparameters that are increased after each subproblem. We consider a subproblem "solved" when $\mathcal{L}_{\text{ELBO}}$ stops increasing. We follow Nemirovsky (1999) and previous work (Lachapelle et al., 2019; Yu et al., 2019) in the update schedule for α_t and ρ_t . We initialise $\rho_0 = 0$ and α_0 heuristically such that the value of $\alpha_0 |h(\mathbf{A}_{\boldsymbol{\theta}})|^2$ is a fraction of the scale of $\mathcal{L}_{\text{ELBO}}$. The scale of $\mathcal{L}_{\text{ELBO}}$ can be found by simply running the GP-CDEs without the causal component. After each subproblem we update

$$\rho_{t+1} \leftarrow \rho_t + \alpha_t h(\mathbf{A}_{\boldsymbol{\theta}_t}), \quad (25)$$

$$\alpha_{t+1} \leftarrow \begin{cases} \nu \alpha_t & \text{if } h(\mathbf{A}_{\boldsymbol{\theta}_t}) > \gamma h(\mathbf{A}_{\boldsymbol{\theta}_{t-1}}) \\ \alpha_t & \text{Otherwise} \end{cases} \quad (26)$$

where we set $\nu = 10.0$ and $\gamma = 0.9$. Optimisation is stopped when $h(\mathbf{A}_{\boldsymbol{\theta}_t}) < \epsilon$.

As Gaussian process models with latent variables suffer from local minima, we found that breaking up training into phases aided the optimisation. We also outline other choices that helped.

Warm up phase: This phase of training was the first subproblem ($t = 0$) of eq. (24). As the hyperparameters of kernels of Gaussian processes can take a while to converge to a solution, we found making this phase of training longer than necessary helpful. We achieved this by ensuring training took at least T_0 iterations before checking if the first subproblem was solved. The value of T_0 will depend on the problem at hand, but for our experiments, $T_0 = 30,000$ sufficed.

Acyclic constraint phase: This is the main part of the training, where the loss described in eq. (24) is optimised. This phase is terminated when $h(\mathbf{A}_{\boldsymbol{\theta}_t}) < \epsilon$.

Cool down phase: The value of the ELBO found at the end of training (when $h(\mathbf{A}_{\theta_t}) < \epsilon$) is highly dependent on how many subproblems the method had to solve. To allow for the comparison of ELBO values across runs (see appendix B.4) we continue training the found acyclic DAG for T_f iterations. This ensured that the found ELBO approximates the ELBO of the final resultant DAG. As some hyperparameters may have been pushed to extreme values by the acyclic threshold if competing with an anticausal edge, we reinitialise the hyperparameters of the edges that are still active to their initial value. This reduces the number of iterations needed for the cool down phase. We found that $T_f = 30,000$ cool down iterations sufficed here.

Thresholding: The values of the hyperparameters can remain very low but the function learnt will still be constant. Following previous work (Lachapelle et al., 2019), to aid with learning the adjacency matrix, we threshold values of hyperparameters to 10^{-15} if they become lower than 10^{-4} after the warm up phase.

Cool down thresholding: Before the start of the cool-down phase, as the values of the hyperparameters sometimes are not exactly 0 due to numerical precision, we find the adjacency matrix with an extra thresholding step. Following Lachapelle et al. (2019), we threshold weights to 0, starting with the lowest weight, until the adjacency is exactly acyclic ($h(\mathbf{A}_{\theta_t}) = 0$).

Final matrix thresholding: To extract the causal graph at the end of training, we remove any edges where the hyperparameters do not encode correlation. To do this, we threshold the linear variances to 10^{-4} and the graph parameters to 0.05, which corresponds to a lengthscale of 20.

B.4. Random Restarts

The main principle behind our method is to find the graph that maximises the marginal likelihood (or a lower bound to it). Maximising the ELBO with respect to the hyperparameters Λ in Gaussian process models is known to suffer from local optima issues (Rasmussen, 2003, Ch. 5). The final hyperparameters found, and hence the adjacency matrix, can be dependent on the initialisation of the hyperparameters. To mitigate this, we use a widely adopted technique of performing random restarts (Dhir et al., 2024). We optimise the loss \mathcal{L} starting from multiple initialisations (this can be done in parallel) N_r times. Then we pick the graph that achieves the highest $\mathcal{L}_{\text{ELBO}}$ as the candidate for the most likely graph. Adding more random restarts for the CGP-CDE should improve performance, as shown for the DGP-CDE appendix C.1.

Algorithm 1 Optimisation procedure for the Causal GP-CDE.

Input: Data \mathbf{X} , number of random restarts N_r , α_0, ρ_0 , initial $\Lambda = \{\theta, \sigma\}$

Result: Most likely adjacency matrix \mathbf{A}^*

Initialise empty list *graphscore* **for** $i = 1$ **to** N_r **do**

for $j = 1$ **to** T_0 **do**

 | Update q, Λ by maximising \mathcal{L} (eq. (24))

end

$t \leftarrow 0$ **while** $h(\mathbf{A}_{\theta_t}) > \epsilon$ **do**

if \mathcal{L} is increasing **then**

 | Update q, Λ by maximising \mathcal{L} (eq. (24))

else

 | $t \leftarrow t + 1$ $\alpha_t \leftarrow \alpha_{t+1}$ $\rho_t \leftarrow \rho_{t+1}$

end

end

 Set α_t, ρ_t to 0 Threshold \mathbf{A}_{θ_t} starting from lowest weight until $h(\mathbf{A}_{\theta_t}) = 0$ **for** $k = 1$ **to** T_f **do**

 | Update q, Λ by maximising \mathcal{L} (eq. (24))

end

 Append $(\mathbf{A}_{\theta}, \mathcal{L})$ to *graphscore*.

end

$\mathbf{A}^* \leftarrow \mathbf{A}_{\theta}$ from *graphscore* with the maximum \mathcal{L} .

B.5. Hyperparameter Priors

As discussed in subsection 3.3, we can place priors on the graphs by placing priors on the hyperparameters θ of the CGP-CDE. For our implementation, we place a prior on θ that favours sparser graphs. Specifically, we use the Gamma prior

$P(\boldsymbol{\theta}) = \text{Gamma}(\eta, \beta)$, where η is the shape parameter and β is the rate parameter. For all experiments, we set $\eta = 1$ and $\beta = 10$. Our hyperparameters for the priors were heuristically chosen and give log probabilities that are a fraction of the rest of the loss.

B.6. Implementation Details

In this section, we outline the details of our implementation.

Hyperparameter initialisations We initialise the hyperparameters $\boldsymbol{\theta} \sim \text{Uniform}(0.01, 1)$, except $\theta_{\text{lin}} = 0.25$. All kernel variances $\boldsymbol{\sigma}$ are initialised to 1 so they all have the same initial weighting and likelihood variance initialised as $\phi^2 = \frac{1}{\kappa^2}$ where $\kappa \sim \text{Uniform}(50, 100)$. The a term in the rational quadratic kernel is initialised as $a \sim \text{Uniform}(0.1, 10)$.

Variational parameters We use 400 inducing points for all datasets as we found this a reasonable trade off between computation time and accuracy. We initialise our inducing point locations at a subset of the data inputs. We use a mutlilayer perception for the latent variable encoder, as described in appendix B.2, with hyperparameters listed in table 2. The encoder weights are initialised from a truncated normal distribution centred on 0 with a standard deviation of $\sqrt{\frac{2}{\text{hidden layer size}}}$ (He et al., 2015).

Loss calculation We use a minibatch size of 128 to calculate the loss. We take 100 Monte Carlo samples to integrate out the latent variables $\mathbf{w}_i = \mathcal{N}(\mu_i, \Sigma_i)$.

Subproblem convergence There are many different ways of measuring convergence. We assume a subproblem to have converged when the difference between the mean of the lower bound for the last t_{conv} steps and the mean of the lower bound for the last $0.5t_{\text{conv}}$ steps is smaller than the standard deviation of the losses for the last t_{conv} . We set $t_{\text{conv}} = 2000$.

Acyclic constraint convergence We stop the constrained optimisation and move onto the cool-down phase when the $h(\mathbf{A}_{\boldsymbol{\theta}_t}) < 10^{-8}$.

Optimisers Each optimisation step consists of two steps. First, we optimise the variational parameters using natural gradients (Salimbeni et al., 2018), with a step size of 0.1. Second, we optimise the Gaussian process hyperparameters using Adam (Kingma and Ba, 2014). For the warm up phase, we use a learning rate of 0.05, for the constrained optimisation phase we use a learning rate of 0.01 if $h(\mathbf{A}_{\boldsymbol{\theta}_t}) > 0.1$ else we use 0.005. In the cool-down phase, we use a learning rate of 0.01.

Random restarts We did as many random restarts as we had computational resources for. This means we did 3 restarts for the three-variable dataset, 5 restarts for the 10-variable synthetic ER and SF datasets, 15 restarts for Sachs and between 2 and 5 restarts for the Syntren graphs.

C. DGP-CDE Details

In section 5.1 we introduce the discrete Gaussian process conditional density estimator (DGP-CDE), which is used to enumerate every possible causal structure for the 3 variable case. For this, a separate DGP-CDE is trained for each of the 25 possible causal graphs, with the Gaussian process prior for each variable defined in eq. (8). The DGP-CDE differs from the CGP-CDE in that it only takes $\mathbf{X}_{\text{PA}_{\mathcal{G}}(i)}$ as inputs, whereas the CGP-CDE takes $\mathbf{X}_{\rightarrow i}$ as inputs and then learns the adjacency matrix.

As the adjacency matrix is fixed for the DGP-CDE there is no acyclic penalty, so the loss function is just the lower bound $\mathcal{L}_{\text{ELBO}}(q, \boldsymbol{\Lambda}, \boldsymbol{\phi}) := \sum_{i=1}^D \mathcal{F}_i(q_i, \boldsymbol{\Lambda}_i, \phi_i)$. When all 25 separate DGP-CDE models have been trained, the most likely graph is selected by choosing the model with the highest marginal likelihood.

C.1. Implementation Details

Loss Calculation As the DGP-CDE is limited in the number of variables it can model by the need to enumerate over all graphs, there is no need to make the lower bound scalable using the methods discussed in appendix B.2 (Hensman et al., 2013). Instead, we use the collapsed version of the lower bound which can be calculated in closed form (Titsias, 2009).

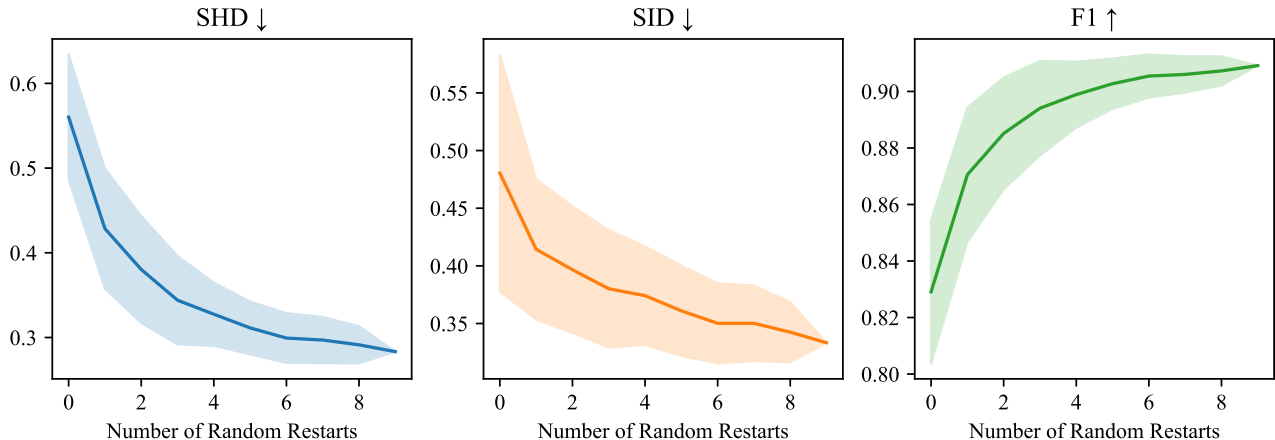


Figure 4. Effect of adding random restarts for the DGP-CDE. We record the metrics (SHD, SID and F1) for the restart with the lowest loss out of a growing set of restarts, starting with one restart and adding one restart at a time. We randomly permute the order in which the random restarts are added 50 times and plot the mean and standard deviation for each of the metrics. This shows that on average increasing the number of random restarts improves performance.

Kernels We use a sum of a linear kernel defined in eq. (13) and a squared exponential kernel defined in eq. (14). This kernel means the kernel expectations needed to calculate the lower bound can be computed in closed form.

Hyperparameters The kernel variances are initialised as $\sigma_i = 1$, the likelihood variance is randomly sampled as $\phi_i^2 \sim \text{Uniform}(10^{-4}, 10^{-2})$ and the precision parameter $\theta_i \sim \text{Uniform}(1, 100)$.

Variational parameters As the enumeration over graphs is computationally expensive, we use 200 inducing points which we found to be sufficient. As we are not using stochastic variational inference (Hensman et al., 2013) for the DGP-CDE, we can no longer mini-batch so don’t use a multilayer perceptron for the latent variables. Instead, we initialise the latent variable mean as $\mu_i = 0.1\mathbf{x}_i$ and standard deviation is randomly sampled $\Sigma_i \sim \text{Uniform}(0, 0.1)$.

Optimisation Schedule The use of the collapsed bound for the DGP-CDE requires a different optimisation schedule than for the CGP-CDE. This consists of a two part optimisation scheme. Due to the loss function being highly non-convex and suffering from local optima, the first step of the optimisation scheme uses Adam (Kingma and Ba, 2014) with a learning rate of 0.05 to get into a good region of the decision space. Once the loss function reaches the value a noise model would have, the optimisation scheme switches to the Broyden-Fletcher-Goldfarb-Shanno (BFGS) algorithm to perform gradient descent for the final part of the optimisation.

Random Restarts We did 10 random restarts for each DGP-CDE, selecting the one with the best lower bound for our final result. We analysed the effect of the random restarts by permuting the order of the random restarts and plotting, in fig. 4, the mean and standard deviation of the SHD, SID and F1 across permutations as the number of restarts increases. From the plot, it is clear that as the number of random restarts increases, the mean value of the metrics, on average, improves. This is because more random restarts allow a more thorough exploration of the loss function. It also shows that a higher value of $\mathcal{L}_{\text{ELBO}}$ does lead to better causal structure discovery.

D. Data Standardisation

For additive noise models, it has been shown that when data is sampled from a simulated DAG and not normalised, the marginal variance tends to increase along the causal order (Reisach et al., 2021). When this is the case, it is possible to, at least partially, determine the causal order by ranking the marginal variance of variables. Reisach et al. (2021) demonstrate that commonly used synthetic datasets often have this property meaning a simple baseline method based on variance sorting and regression can perform as well as some recent continuous structure learning algorithms. This variance can be manipulated by rescaling (such as changing measurement units), which would then give a different causal order. As

such, results that take advantage of the variance may be sensitive to measurement scales. Such effects may also persist in real-world datasets due to the measurement scale used.

To get rid of these effects, we standardise all datasets before applying any of the causal discovery methods discussed in this paper. This means our results for the baselines don't match the results reported in the original papers for similar datasets (Montagna et al., 2023; Lachapelle et al., 2019; Rolland et al., 2022) (note that some of these works also define SHD of an anti-causal edge as 1 where we define it as 2).

E. Data Generation Details

3 Variable Synthetic Data: For each of the six distinct causal structures for three variables (up to permutations of the variables) we generated five datasets, each with 1000 samples. The data was generated by fitting a GP-CDE with a sum of a linear kernel and one other kernel randomly selected out of Matérn12, Matérn32, Matérn52, squared exponential and rational quadratic. The kernel hyperparameters are sampled from $\sigma_i \sim \text{Uniform}(\mathbf{1}, \mathbf{100})$ and $\theta_i \sim \text{Gamma}(\mathbf{1.5}, \mathbf{1})$ while the other parameters are sampled as $\phi_i \sim \text{Uniform}(\mathbf{0.01}, \mathbf{1})$ and $\mathbf{w}_i \sim \mathcal{N}(\mathbf{0}, \mathbf{1})$. The data is then sampled from this GP-CDE.

10 Variable Synthetic Data: For each of the ER (Erdos et al., 1960) and SF (Barabási and Albert, 1999) sampling schemes, we generate five random 10 node graphs, with an expected number of edges of 15 to ensure the graph is not too sparse or dense. Data is then generated for each node X_i using

$$X_i := f_i^{NN}(\mathbf{X}_{\text{PA}_{\mathcal{G}}(i)}, \epsilon_i),$$

where $\text{PA}_{\mathcal{G}}(i)$ are the parents of X_i and $\epsilon_i \sim \mathcal{N}(0, 1)$ is sampled from $\epsilon_i \sim \mathcal{N}(0, 1)$. f^{NN} is a randomly initialised neural network with two layers, 128 units and ReLU activation functions. For each graph, we sample 1000 data points.

Syntren Dataset: Syntren is a synthetic data generator that approximates real transcriptional regulatory networks (Van den Bulcke et al., 2006). Networks are selected from previously described transcriptional regulatory networks. Relationships between the genes are based on the Michaelis-Menten and Hill enzyme kinetic equations. The kinetic equations contain some biological noise and some lognormal noise is added on top. We use the data generated by Lachapelle et al. (Lachapelle et al., 2019). This contains 10 datasets of 500 samples, each with 20 nodes. The data was generated using the syntren data generator (Van den Bulcke et al., 2006), using the E.coli network with the default parameters except for the *probability for complex 2-regulator interactions* which was set to one (Lachapelle et al., 2019).

Sachs Dataset: The Sachs dataset is a real-world dataset containing 11 nodes and 853 observations measuring the expression levels of proteins (Sachs et al., 2005). While Sachs et al. provide a consensus graph based on domain knowledge (Sachs et al., 2005), it contains cycles and there is some debate around its validity (Mooij et al., 2016). This has led to causal discovery methods using different ground truth graphs, for example, Yu et al. use a ground truth graph with 20 edges while Lachapelle et al. and Montagna et al. use a ground truth graph with 17 edges (Yu et al., 2019; Lachapelle et al., 2019; Montagna et al., 2023). Given the uncertainty around the correct causal graph, we use the 17 edge graph used by Lachapelle et al. (Lachapelle et al., 2019) for the results presented in this paper as it is commonly used. However, we found CGP-CDE outperformed, or performed similarly in some metrics, to the other baselines for other widely used ground truth graphs.

F. Details about Baselines

For SCORE (Rolland et al., 2022) and NoGAM (Montagna et al., 2023) we use the implementation in the dodiscover package <https://github.com/py-why/dodiscover>. For CAM (Bühlmann et al., 2014), NOTEARS (Zheng et al., 2018), GraN-DAG and GraN-DAG++ (Lachapelle et al., 2019) we use the implementations in the GraN-DAG github repository <https://github.com/kurowasan/GraN-DAG>.

SCORE & NoGAM: SCORE and NoGAM have very similar hyperparameters and for both methods, we use the default values ridge regression suggested by Montagna et al. which they tuned to minimise the generalisation error on the estimated residuals (Montagna et al., 2023). We also use the default values for both methods for all the hyperparameters for the Stein gradient and Hessian estimators and CAM pruning step except for the cutoff value for the CAM pruning step which we set to 0.01 as is standard for CAM and follows Montagna et al. (Montagna et al., 2023). NoGAM has the additional hyperparameter of *number of cross validation models*, for which we use the preset value of five.

CAM: For CAM we use the default preliminary neighbourhood selection and DAG pruning methods and a cutoff value of 0.001 for the edge pruning as suggested by the authors (Bühlmann et al., 2014).

NOTEARS: For NOTEARS we again use the default values, including a threshold of 0.3 as is suggested as a reasonable choice by Zheng et al. (Zheng et al., 2018). We also use the default values suggested by Lachapelle et al. (Lachapelle et al., 2019) for the augmented Lagrangian.

GraN-DAG & GraN-DAG++: GraN-DAG and GraN-DAG++ have the same hyperparameters, for which we use the values selected by the authors based on small scale experiments on a single dataset generated from a 10 node ER graph (Lachapelle et al., 2019). This includes setting each neural network to have 10 units and leaky-ReLU activation functions. We use the same number of hidden layers for each dataset as the authors, who use two hidden layers for ER and SF graphs and one hidden layer for the Sachs and Syntren datasets. We run both these methods with preliminary neighbourhood search and pruning, as is shown to be effective in reducing overfitting (Lachapelle et al., 2019). We also follow the authors in using a batch size of 64. For both GraN-DAG and GraN-DAG++ we use the preset values for the augmented Lagrangian (Lachapelle et al., 2019).

G. Computational Resources

The experiments in this paper were run on 4090 GPUs which have 24GB of memory.